Received: 15 October 2019 | Revised: 14 December 2019 | Accepted: 7 April 2020

DOI: 10.1002/aic.16247

AIChE JOURNAL

SEPARATIONS: MATERIALS, DEVICES AND PROCESSES

High-performance oxygen transport membrane reactors integrated with IGCC for carbon capture

Lili Cai[1] | Xiao-Yu Wu[2] | Xuefeng Zhu[1,3,4] | Ahmed F. Ghoniem[2] | Weishen Yang[1,3]

[1]State Key Laboratory of Catalysis, Dalian Institute of Chemical Physics, Chinese Academy of Sciences, Dalian, China

[2]Department of Mechanical Engineering, Massachusetts Institute of Technology, Cambridge, Massachusetts

[3]University of Chinese Academy of Sciences, Beijing, China

[4]Dalian National Laboratory for Clean Energy, Chinese Academy of Sciences, Dalian, China

Correspondence
Xuefeng Zhu, State Key Laboratory of Catalysis, Dalian Institute of Chemical Physics, Chinese Academy of Sciences, 457 Zhongshan Road, Dalian 116023, China.
Email: zhuxf@dicp.ac.cn

Funding information
Chinese Academy of Sciences, Grant/Award Number: XDB17000000; Dalian Institute of Chemical Physics, Grant/Award Numbers: DICP&QIBEBT UN201708, DNL180203; National Natural Science Foundation of China, Grant/Award Numbers: 21776267, U1508203; Liaoning Revitalization Talents Program, Grant/Award Number: XLYC1801004; Exelon Corporation

Abstract

Precombustion carbon capture is an effective strategy to reduce large-scale CO_2 emissions, which is mainly used in the area of integrated gasification combined cycle (IGCC) power plants. Oxygen transport membranes (OTMs) were suggested as the air separation unit to produce high purity oxygen for the gasifier. However, the improvement in efficiency was limited. Here, a new IGCC process is reported based on a robust OTM reactor, where the OTM reactor is used behind the coal gasifier. This IGCC-OTM process fulfills syngas oxidation, H_2 production, and carbon capture in one unit, thus a significant decrease of the energy penalty is expectable. The membrane reactor does not use noble metal components, and exhibits high hydrogen production rates, high hydrogen separation factor (10^3–10^4), and stable performance in a gas mixture mimicking real syngas compositions from a coal gasifier with H_2S concentrations up to 1,000 ppm.

KEYWORDS

carbon capture (CC), hydrogen production, IGCC, membrane reactor, oxygen transport membrane (OTM)

1 | INTRODUCTION

Greenhouse gas emission and accumulation in the atmosphere and global climate change are linked. More than 30% of the global CO_2 emission comes from fossil fuels power plants.[1-3] Three promising routes for CO_2 capture in these plants: pre- and postcombustion capture and oxy-fuel combustion, are under development. Among them, the integrated gasification combined cycle (IGCC) with carbon capture (CC) shows great potential as a precombustion capture technology.[4-6] However, an efficiency reduction of 8–12% points has been predicted; when using a water gas shift (WGS) reactor with absorption-based CO_2 capture technologies (IGCC-WGS), compared with the cycles without CC.[7-9] The high-temperature gasification (1,200–1,400°C) and low-temperature CO_2 separation (25–400°C) make heat integration inefficient, and lead to excessive exergy loss. H_2/CO_2 separation and CC based on the state-of-the-art absorption (e.g., amine and ammonia)[10] or adsorption processes (e.g., zeolites,[11,12] activated carbon[13]) consume much energy and significantly decreases the net output of the power plants.

Several membrane technologies were proposed to integrate with IGCC to decrease the energy penalty associated with CC. There are generally two approaches. First, membranes, usually oxygen transport membranes (OTMs), are used in the air separation unit to produce high purity oxygen for the gasifier.[14] However, the efficiency improvement is limited, around 1% point.[15,16] The second approach is to use membranes for hydrogen separation/production, replacing the CO_2 separation unit, which accounts for more than 50% of the CC-related auxiliary load of the IGCC.[17] Many types of membranes have been proposed to fulfill hydrogen separation from the products of

Lili Cai and Xiao-Yu Wu contributed equally to this work.

water gas shifting (WGS) reaction in IGCC process, such as Pd-based composite membranes,[18] polymer membranes,[19,20] and dense proton-conducting membranes.[21-25] However, challenges in the cost and stability issues still hinder their applications in the IGCC process. Therefore, more efforts should be focused on developing an ideal hydrogen production membrane reactor for IGCC, which was operated at a temperature close to that of the gasifier, has fast separation kinetics, uses earth-abundant elements, and has long-term stability in a gas mixture containing H_2, H_2O(g), CO, CO_2, and H_2S.

OTM reactors have been studied for different applications, such as partial oxidation of methane and other light alkanes,[26,27] oxidative dehydrogenation of alkanes,[28-30] methane aromatization,[31] and hydrogen separation/production.[32-39] Praxair Inc. has made great progress on the commercialization of the OTM reactor for the conversion of natural gas to syngas. They started a project to produce 9,940 N m^3 hr^{-1} syngas for a methanol plant using an OTM reactor in 2019.[40,41] In the hydrogen separation/production application, two sides of the OTM are both under strong reducing atmospheres. The stability of OTM is more crucial than that in air separation applications. In previous studies, many stable OTM materials were developed in these harsh conditions. Among them, OTMs, including $BaCo_xFe_yZr_{1-x-y}O_{3-\delta}$,[32,33] $La_{0.9}Ca_{0.1}FeO_{3-\delta}$,[34] $Ce_{0.85}Sm_{0.15}O_{1.925}$–$Sm_{0.6}Sr_{0.4}Al_{0.3}Fe_{0.7}O_{3-\delta}$,[35] $Ce_{0.85}Sm_{0.15}O_{1.925}$–$Sr_2Fe_{1.5}Mo_{0.5}O_{6-\delta}$,[36] and $Ce_{0.85}Sm_{0.15}O_{1.925}$–$Sm_{0.6}Sr_{0.4}Cr_{0.3}Fe_{0.7}O_{3-\delta}$,[38] exhibited outstanding stabilities. These materials may be appropriate for H_2 production in the IGCC process.

In this study, we report on a novel precombustion CC concept by integrating IGCC with a high-temperature OTM reactor, IGCC-OTM. The traditional IGCC with CC process includes coal gasifier, WGS reactor, acid gas removal unit, CO_2 capture unit, and combustion and power generation unit. In the new IGCC-OTM process, the OTM reactor is placed downstream of the coal gasifier. The syngas from the gasifier and steam are supplied to the two sides of OTM, separately. High concentration CO_2 produced from syngas full oxidation is ready for capture and storage. On the other side, the produced hydrogen from water dissociation and the unconverted steam flow to the combustion and power generation unit. This IGCC-OTM process fulfills syngas oxidation, H_2 production, and CC in one unit, simplifies the overall process and improves the heat integration. Thus, a significant decrease of the energy penalty due to CC is expected. Different from other H_2 separation membranes, the OTM only allows the oxygen ions produced by water dissociation reaction to be transported to the syngas side by potential gradient across the membrane. Thus, the theoretical hydrogen selectivity is 100%. If the unreacted steam is removed, high-purity hydrogen can be obtained. Meanwhile, previous studies have verified that the OTM reactor has good stability for hydrogen production under various atmospheres.[34-38] In this article, our experimental results show that this novel OTM reactor with non-precious metal catalysts shows promising results in converting syngas to water and CO_2, with hydrogen production rates comparable to state-of-the-art Pd-based composite membranes, high hydrogen separation selectivity (separation factor 10^3–10^4), and stable performance in an environment containing H_2, H_2O(g), CO, CO_2, and 1,000 ppm H_2S. These results indicate that the developed OTM reactor is possible to be used in the IGCC-OTM process.

2 | EXPERIMENTAL

2.1 | Materials

The methods used for the preparation of 10 wt% $Ni/Sm_{0.15}Ce_{0.85}O_{2-\delta}$ (SDC) catalysts and 75 wt% $Sm_{0.15}Ce_{0.85}O_{2-\delta}$–25 wt% $Sm_{0.6}Sr_{0.4}Cr_{0.3}Fe_{0.7}O_{3-\delta}$ (SDC-SSCF) membranes and bars were described in previous studies[26,36] and provided in the Supporting Information.

2.2 | Treatment of membrane material and catalyst under different atmospheres

SDC-SSCF or Ni/SDC particles (0.5 g, 20–60 mesh) were packed in fixed-bed reactors and calcined under atmospheres of 10% CO_2 (volume ratio) or 100 ppm H_2S (10% H_2O(g), 50% H_2 and He balance) at 900°C for 10 hr. The reactors were cooled to room temperature at the same atmospheres. The total flow rates of the mixtures were kept at 100 ml min^{-1}. The particles after treatment were ground to powders and characterized by X-ray diffraction (XRD).

2.3 | Conductivities of materials

Conductivities of the samples were measured by the four-probe method on the sintered bars under different conditions. During the tests, a constant current was applied to the samples with an electrochemical workstation (Princeton Applied Research 263A). The voltages were measured by a Keithley 2000 multimeter. The total conductivities were measured at 950–600°C under atmospheres of 80% H_2–20 H_2O(g) and 20% H_2–80 H_2O(g), respectively. The cooling rates were set at 1°C min^{-1}. The total flow rates of the gas mixtures were 200 ml min^{-1}.

2.4 | Test of membrane reactors

The homemade apparatus for hydrogen production membrane reactor is similar to that in previous publications.[35,36] Gas-tight membranes were sealed with silver rings onto alumina tubes. All the effective membrane areas were in the range of 0.7∼0.9 cm^2. On the H_2O(g) side (Figure 1, Side II), the concentration of steam was slowly increased to 90% (volume ratio) with He balanced ($f_{He,\ in}$). Then, different amounts of H_2 and N_2 mixed gas were supplied to the H_2 side (Side I). The effluent ($f_{He,\ out}$) on the H_2O(g) side was cooled and dried before tested in a gas chromatograph (Agilent 6890A), which equipped with Porapak Q and 13X columns. The effect of hydrogen concentration (total flow rates were kept at 100 ml min^{-1}) and the flow rates of H_2–N_2 (H_2/N_2 = 1/1) mixtures on Side I, and the flow

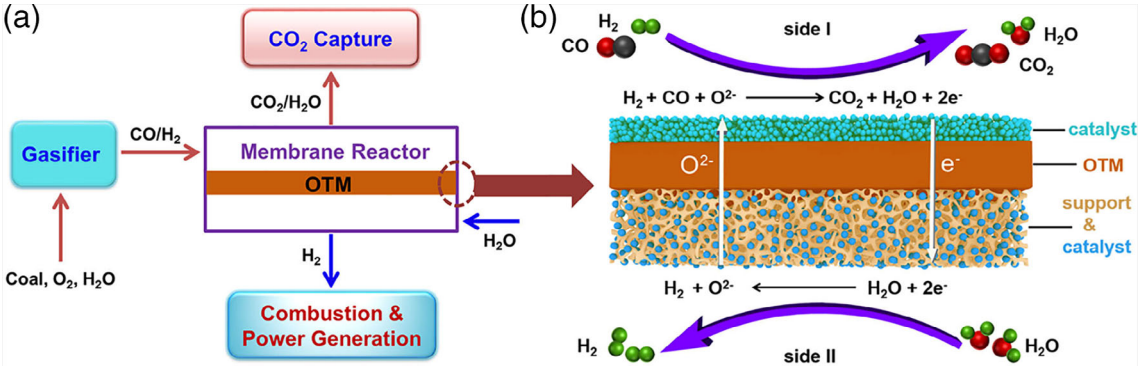

FIGURE 1 The scheme of the novel IGCC-OTM process. (a) Illustration of the IGCC-OTM process. (b) Coupling H_2 production, syngas oxidation, and carbon capture in an OTM reactor. IGCC, integrated gasification combined cycle; OTM, oxygen transport membranes [Color figure can be viewed at wileyonlinelibrary.com]

rates of H_2O(g)–He (90% H_2O) mixtures on Side II (50 ml min^{-1} H_2–50 ml min^{-1} N_2 on Side I) were tested.

Syngas with H_2/CO molar ratio of 1 was fed to the Side I to test the performance of the membrane reactor for hydrogen production and syngas conversion. The influence of flow rate of syngas on the performance of hydrogen production was measured; when the atmospheres of Side II of the membrane were fixed at 180 ml min^{-1} H_2O(g) – 20 ml min^{-1} He. The influence of temperature on the performance of hydrogen production rates was measured; when the atmospheres of two sides of the membrane were fixed at 180 ml min^{-1} H_2O(g) – 20 ml min^{-1} He and 50 ml min^{-1} H_2 – 50 ml min^{-1} CO, respectively. The stability of the membrane was tested at 900°C under atmospheres containing different concentrations of H_2, CO, CO_2, and H_2S.

The H_2 production rates (F_{H_2}) and separation factors (α) were calculated according to the following equations, where S is the effective membrane areas; y_{N_2} and y_{H_2} represent the concentrations of N_2 and H_2 on Side II, respectively; x_{N_2} and x_{H_2} represent the concentrations of N_2 and H_2 on Side I, respectively.

$$F_{H_2} = \frac{(f_{He,out} - f_{He,in})}{S}. \quad (1)$$

$$\alpha\left(\frac{H_2}{N_2}\right) = \frac{\left(\frac{y}{y_{N_2}}\right)}{\left(\frac{x_{H_2}}{x_{N_2}}\right)}. \quad (2)$$

2.5 | Membranes and catalysts characterization

XRD measurements were operated on an Empyrean-100 instrument (Cu Kα radiation, 40 kV and 40 mA) with a step width of 0.02°. Scanning electron microscopy images and energy dispersive X-ray (EDX) mapping spectroscopies were obtained on a Quanta 200 FEG instrument (FEI Company). High resolution transmission electron microscopy images were observed on TECNAI G2 F30 (FEI Company) and JEM-ARM200F (Japan). Brumauer–Emmett–Teller (BET) surface areas of the catalysts were calculated from the N_2 adsorption isotherms (Micromeritics ASAP 2020 PLUS HD88).

3 | RESULTS AND DISCUSSION

3.1 | IGCC-OTM concept

As discussed earlier, the novel IGCC-OTM process can integrate syngas oxidation, H_2 production, and CC in one unit, as shown in Figure 1. The syngas from the coal gasifier is fed to one side (Side I) of the OTM reactor, and steam is fed to the other (Side II). At elevated temperatures (700–1,000°C), steam combines with electrons and splits into hydrogen and oxygen ions. Oxygen ions diffuse across the membrane to Side I and oxidize the syngas into water and CO_2, and generate electrons that return to Side II. Hydrogen from water splitting on Side II is used in the combined cycle to generate electricity, while the unconverted steam acts as the diluent to control the combustion temperature. On Side I, H_2S in the raw gas from the gasifier is oxidized to SO_2, and is converted to sulfur via the Claus reaction in the membrane reactor.[42-44] The effluent from that side consists only of H_2O(g), CO_2, and solid sulfur. After condensation, solid separation, and compression, a stream with high purity CO_2 is ready for storage.

3.2 | Properties of membrane and catalyst

A critical element in the IGCC-OTM technology is a stable and low-cost membrane reactor with high permeability and catalytic activity. For this purpose, we constructed a dual-phase OTM of SDC–SSCF and non-noble metal catalysts (10 wt% Ni/SDC). The Ni/SDC catalyst was prepared by an ethylenediamine tetraacetic-citric method with a specific area of 8.5 m^2/g, and contained the NiO and SDC phases (Figure 2a–c). The particle sizes of NiO and SDC are 50–100 nm. The dual-phase membrane material was prepared via a one-pot method at elevated temperature with the two phases formed spontaneously. Both phases show interplanar spacing values similar to those

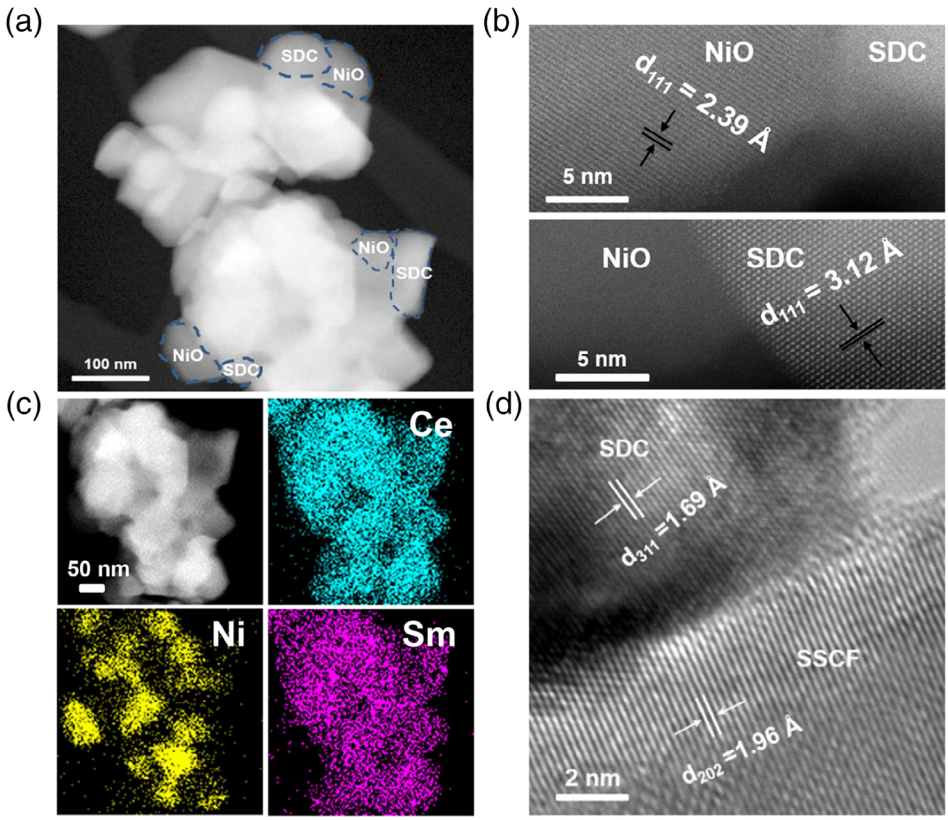

FIGURE 2 HRTEM analysis of the catalyst and membrane. (a, b) HRTEM images and (c) EDX elemental mapping of the Ni/SDC catalyst, (d) HRTEM images of SDC-SSCF membrane. EDX, energy dispersive X-ray; HRTEM, high resolution transmission electron microscopy [Color figure can be viewed at wileyonlinelibrary.com]

corresponding to the single-phase materials (Figure 2d), indicating that they are chemically compatible. SDC–SSCF was fabricated into flat membranes with a thin dense layer and a thick porous support using tape-casting and co-sintering method (Figure S1). The grain size of SDC-SSCF is 0.5–3 μm (Figure 3a), and the thickness of the dense layer is 36 μm (Figure 3b). The 10 wt% Ni/SDC catalysts with a thickness of approximately 20 μm were added on Side I to oxidize H_2 and CO to H_2O(g) and CO_2, respectively. The membrane support on Side II (a porosity of 54% and a thickness of 760 μm) has two functions: serving as a mechanical support (skeleton) to the thin dense separation layer, and accommodating the Ni/SDC catalysts for the water splitting reaction (Figure 3c).

To examine the structural stability of the 10 wt% Ni/SDC catalyst pellets and the SDC–SSCF membrane material, samples were treated in different atmospheres, that is, 10% CO_2 or 100 ppm H_2S (10% H_2O (g), 50% H_2 with He balance) at 900°C for 10 hr. No new peaks were detected using XRD (Figure 4) compared with the ones prepared in air, revealing their good stabilities in H_2, H_2O(g), CO_2, and H_2S mixtures. The membrane material should have both high electronic and ionic conductivities under operation conditions to accelerate the ambipolar diffusion of oxygen ions and electrons through the bulk. The total conductivities of SDC–SSCF were tested in the temperature range of 600–950°C under atmospheres of 80% H_2–20% H_2O(g) and 20% H_2–80% H_2O(g), as shown in Figure 5. The two atmospheres were used to imitate the oxygen partial pressures of the membrane for hydrogen production on both sides, respectively. As shown in Figure 5a, the corresponding oxygen partial pressures increase from 8.1×10^{-26} to 2.5×10^{-17} atm and 2.1×10^{-23} to 7.9×10^{-15} atm as the temperature increases from 650–950°C. The conductivity measurement shows that SDC–SSCF is a mixed ionic and electronic conductor under reducing conditions, which facilitates the charge exchange between the catalyst and membrane. The Arrhenius plots of the conductivities (Figure 5b) indicated that the conductive mechanisms of the SDC–SSCF material in these conditions did not change.

3.3 | Performance of the membrane reactor

We compared the performances of Ni/SDC catalysts on Side II prepared using different methods. In M1 configuration, the Ni precursor was added in the tape-casting slurry with a weight content of 1 wt% in the porous support. Its porosity is about 44%, measured by the Archimedes method. Its morphology is shown in Figure S2a. In the other two configurations, a precursor solution of 10 wt% Ni/SDC was infiltrated into the porous support, which was repeated for 10–20 times until the weight of the membranes increased by approximately 10% (M2, Figure S2b) or 20% (M3, Figure S2c). Meanwhile, the corresponding porosities of M2 and M3 are 40% and 19%, respectively. The hydrogen production performances of these membrane configurations were evaluated in a reactor, first with model fuels and then with fuels similar to the products of coal gasification. Fuel mixtures were fed to Side I and H_2O(g) to Side II. As shown in Figures 6 and S3, important parameters, such as the fuel concentration, flow rates of fuel mixtures and H_2O(g), and temperature, affect the

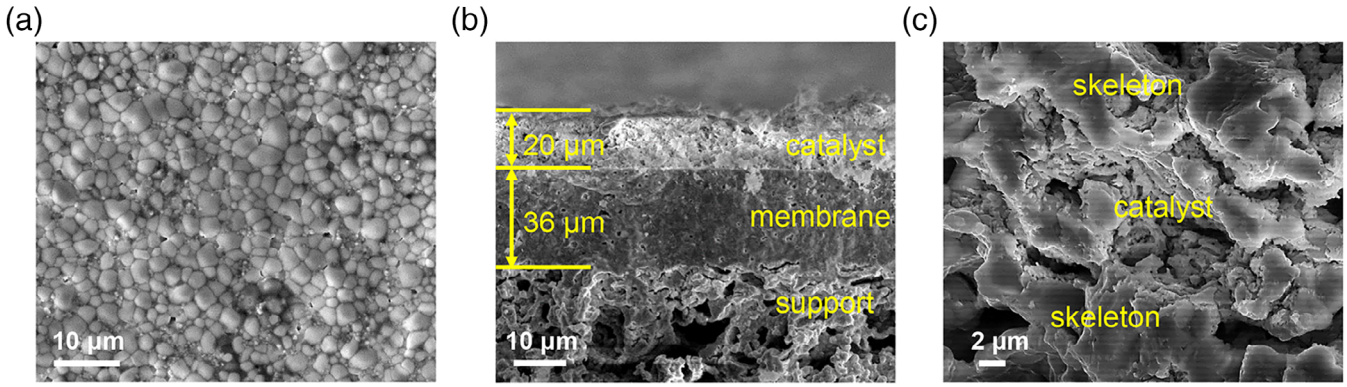

FIGURE 3 SEM images of SDC-SSCF dual-phase membranes. (a) Fresh membrane (top view), and (b, c) membranes with catalysts (cross-section of the M2). SEM, scanning electron microscopy [Color figure can be viewed at wileyonlinelibrary.com]

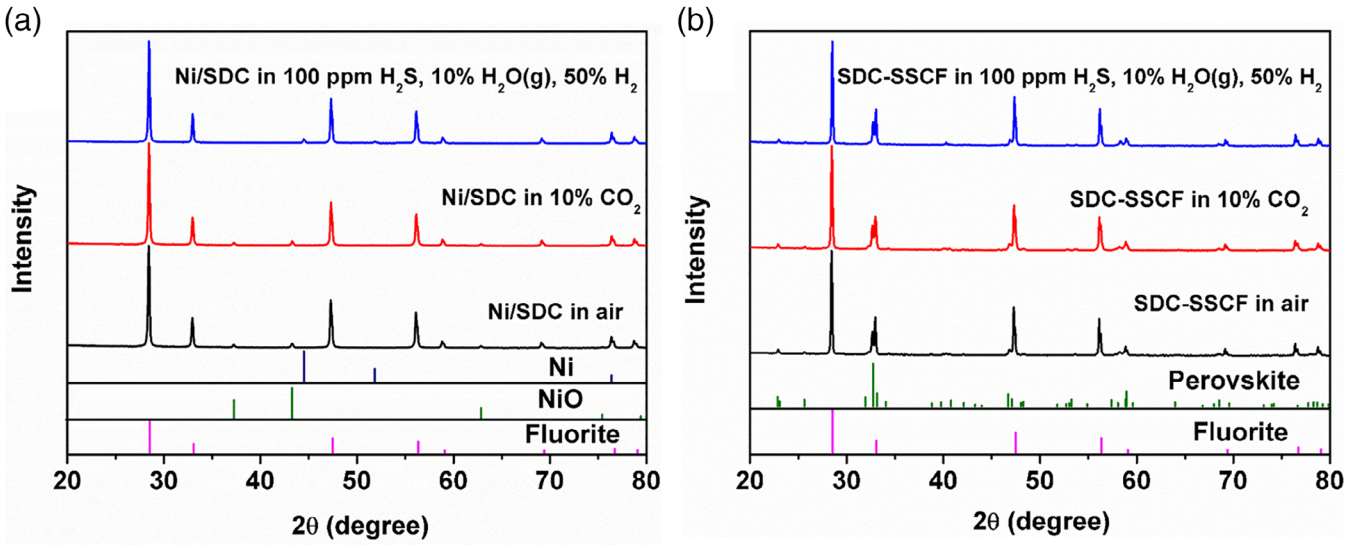

FIGURE 4 XRD patterns of (a) 10 wt% Ni/SDC and (b) SDC-SSCF treated under different atmospheres. The standard JCPDS files for fluorite (CeO_2, PDF#43-1002), Ni (PDF#04-0850), NiO (PDF#47-1049), and perovskite ($FeSmO_3$, PDF#39-1490) are also listed in this figure. XRD, X-ray diffraction [Color figure can be viewed at wileyonlinelibrary.com]

hydrogen production rate on Side II significantly. Hydrogen production rates of all membranes were raised with fuel concentrations (Figure 6a). This is ascribed to the increase in oxygen ionic flux with larger oxygen partial pressure gradient between the two sides of the membrane (Figure S4), which is up to four- to five-orders of magnitude compared to the one-order of magnitude in the hydrogen partial pressure. The higher oxygen partial pressure gradient drives faster oxygen permeation, and hence, much higher hydrogen production rates than proton-conducting membranes under similar conditions, as compared in Table S1. The conversion rates of water were also plotted in Figure 6c. When the flow rate of H_2O(g)-He was 45 ml min^{-1}, the conversion rates of water reached to 17.6%, 20.2%, and 19.2% in M1, M2, and M3 reactors, respectively. The conversion rates of water would not be very high because of the short contact time of reactants with membranes in the disk membrane reactors and limited membrane areas. Higher water conversion rates will be achieved when using tubular membrane reactors under elevated operating pressures.

Temperature is an important factor that affects the hydrogen production process. The critical substeps, including water splitting, hydrogen oxidation reactions, and ambipolar transport of oxygen ions and electrons, are all thermally activated. Below 940°C, the rate on M1 is lower than those on M2 and M3, as the directly added Ni catalysts in the porous support have lower activity in M1.[45-47] The membrane (M3) with more catalysts but lower support porosity (19%) shows lower hydrogen production rates than M2 (40%), which indicates that concentration polarization partially influences the performance. The separation factors under each condition were 10^3–10^4 (Tables S2–S4), showing that the 36 μm dense layer effectively produced high purity hydrogen using the fuel mixture. The hydrogen production rates of M2 are comparable to those of Pd-based membranes (Table S5) but without using precious metals. In addition, the hydrogen production rates and separation factors of M2 are much higher than those of microporous membranes (Table S6).

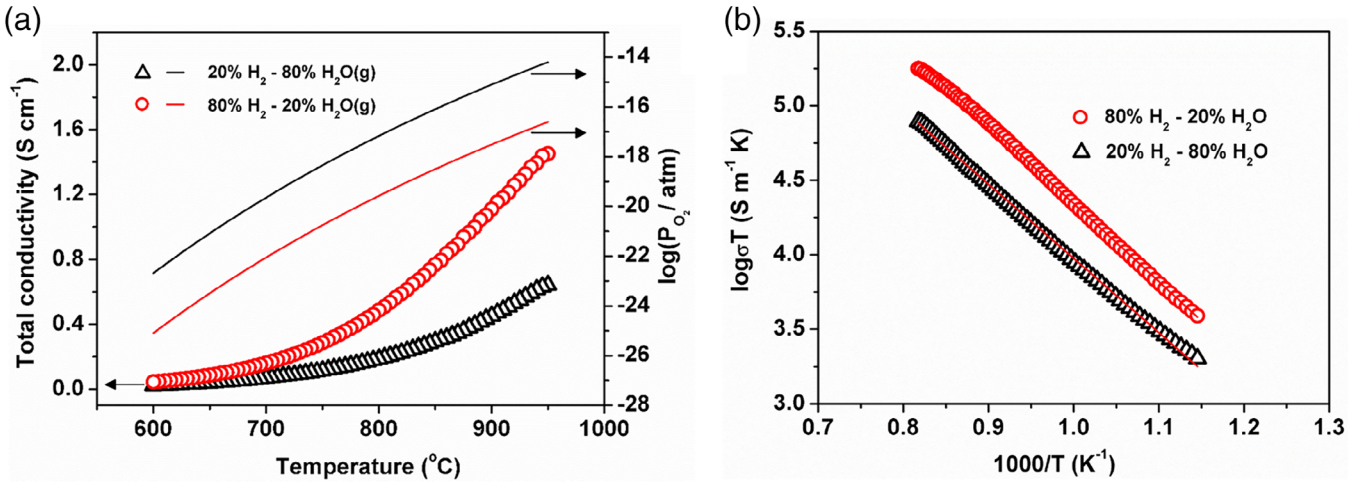

FIGURE 5 Dependence of (a) the total conductivities of SDC-SSCF and the corresponding oxygen partial pressures on temperature under atmospheres of 80% H_2–20% H_2O(g) and 20% H_2–80% H_2O(g). (b) Arrhenius plots of the conductivities. The total flow rate of the gas mixtures was 200 ml min^{-1} [Color figure can be viewed at wileyonlinelibrary.com]

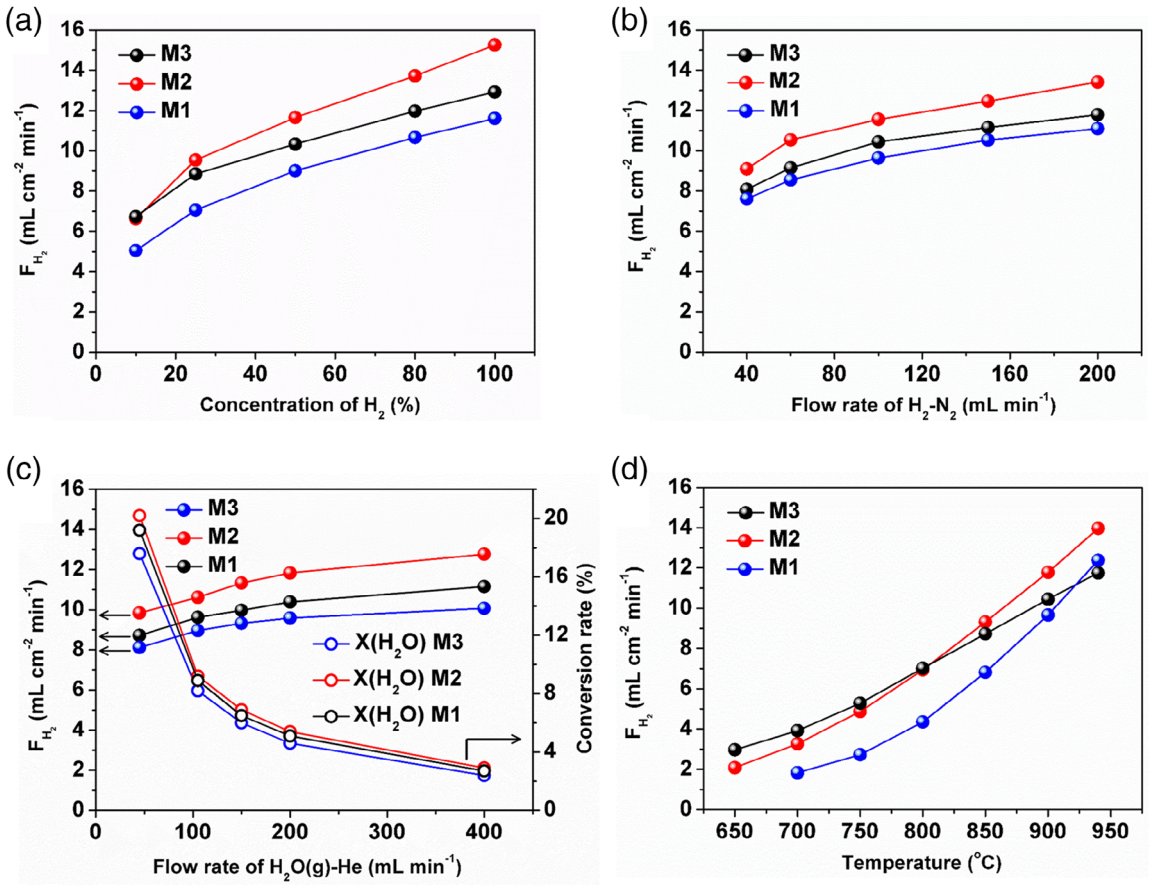

FIGURE 6 Performances of the membranes under different conditions. Dependence of hydrogen production performance on (a) concentration of H_2 at 900°C, (b) flow rate of H_2-N_2 mixture at 900°C, (c) flow rate of H_2O(g)-He mixture at 900°C, and (d) temperature. The concentration of H_2O(g) is 90% in all tests. The gas flow rate on the H_2O(g) side is 200 ml min^{-1} for (a, b, and d); the gas flow rate on the H_2 side is 100 ml min^{-1} for (a, c, and d); the concentration of H_2 is 50% for (b, c, and d). The conversion rates of water are also plotted in (c) [Color figure can be viewed at wileyonlinelibrary.com]

The hydrogen production was demonstrated on membrane configuration M2 with syngas (H_2/CO ratio of 1, close to the syngas composition from a general electric energy [GEE] gasifier) on Side I. The influence of flow rate of syngas and temperature are shown in Figure 7 and S5. The conversion rates of CO, H_2, and H_2O in each operation condition are plotted in Figure 7, which all increase at higher temperatures. The hydrogen production rates increase with increasing flow rates of syngas (Figure 7a) and temperatures (Figure 7b). However, due to the short contact time of the reactant gases in the membrane reactor, the conversion rate of CO cannot reach a high level. Nevertheless, a CO conversion rate of 41% was reached at 900°C, as shown in Figure 7a. The corresponding H_2 and H_2O conversion rates were 54% and 3%, respectively. In principle, the syngas can be completely converted into water and CO_2 with an operation model shown in Figure S6. Our group is working on the reaction in tubular membrane reactors to obtain complete conversion of CO and achieve a high conversion rate of water.

CO_2 and H_2S impurities are poisonous to many OTMs and Pd-based hydrogen-permeable membranes. Here, the stability of the SDC–SSCF membrane (M2 configuration) was evaluated under different atmospheres for 550 hr (Figure 8a). The hydrogen production rate remained constant, yet at different values depending on the atmospheres on Side I. The rate dropped to a stable value as CO_2 was introduced, which is related to the weak and reversible adsorption of CO_2 on membrane surface.[36,48-50] The production rate was fully recovered when CO_2 was removed. The membrane reactor also kept stable performance in H_2S containing environments even when its concentration was increased to 200 ppm, with the balance gas being H_2. Finally, we examined the stability of the membrane reactor with a gas mixture mimicking a real syngas composition from a

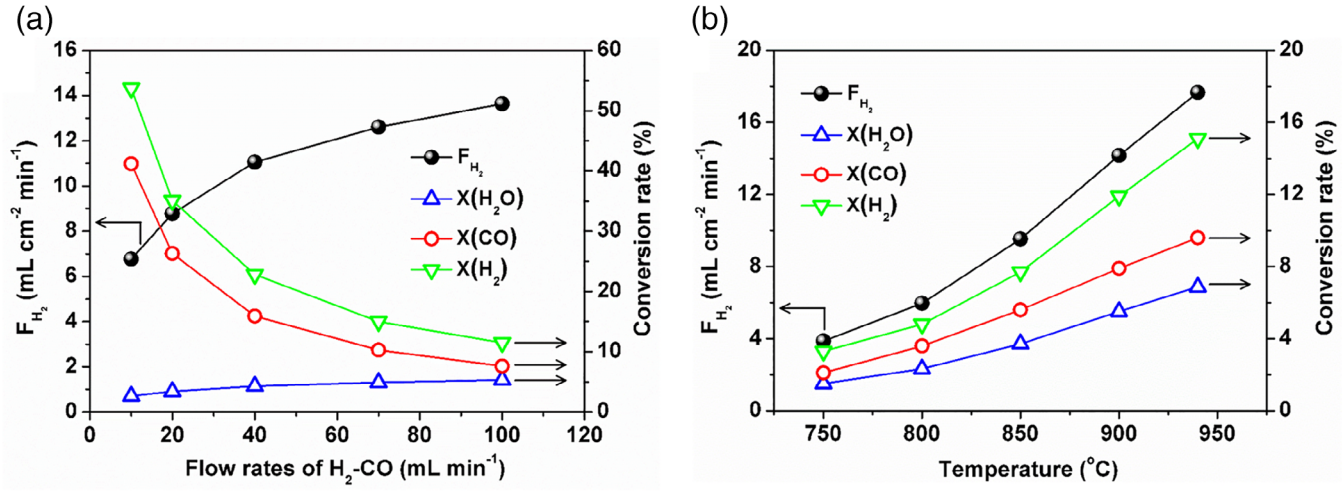

FIGURE 7 Dependences of the hydrogen production rates, and conversion rates of H_2O, H_2, and CO on (a) the syngas flow rate and on (b) temperature for M2 [Color figure can be viewed at wileyonlinelibrary.com]

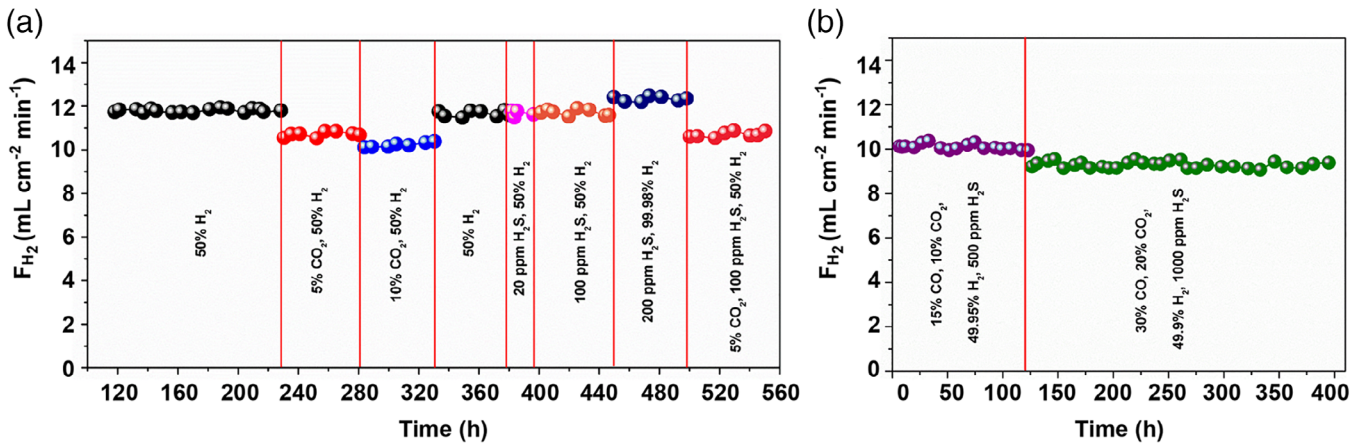

FIGURE 8 The hydrogen production rates during the long-term stability tests of M2 under various atmospheres at 900°C. The flow rate of H_2O(g)–He mixed gas (H_2O(g)/He = 9) was kept at 200 ml min^{-1} on Side II, and the flow rate of fuel mixtures balanced with N_2 was kept at 100 ml min^{-1} on Side I [Color figure can be viewed at wileyonlinelibrary.com]

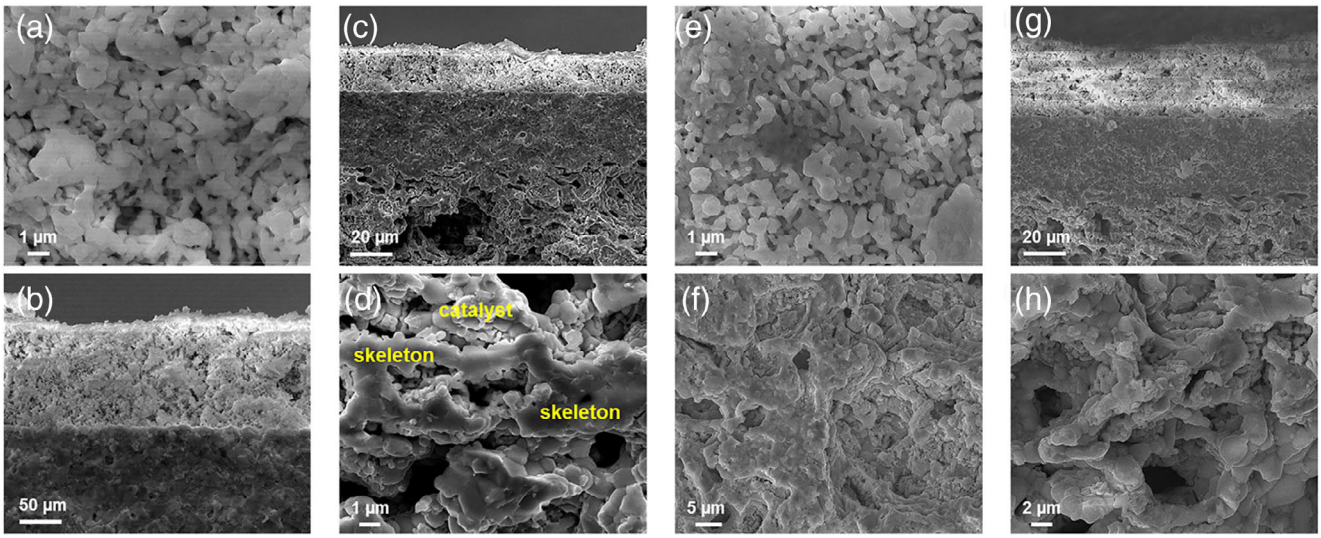

FIGURE 9 SEM images of the spent membranes after long-term stability tests. (a–d) After 550 hr operation (containing 200 ppm H_2S); (e–h) after 400 hr operation (containing 1,000 ppm H_2S); (b, c, and g) cross-section; (a, e, and f) surface section; (a, e) Side I (H_2 side); (d, f, and h) Side II (H_2O(g) side). SEM, scanning electron microscopy [Color figure can be viewed at wileyonlinelibrary.com]

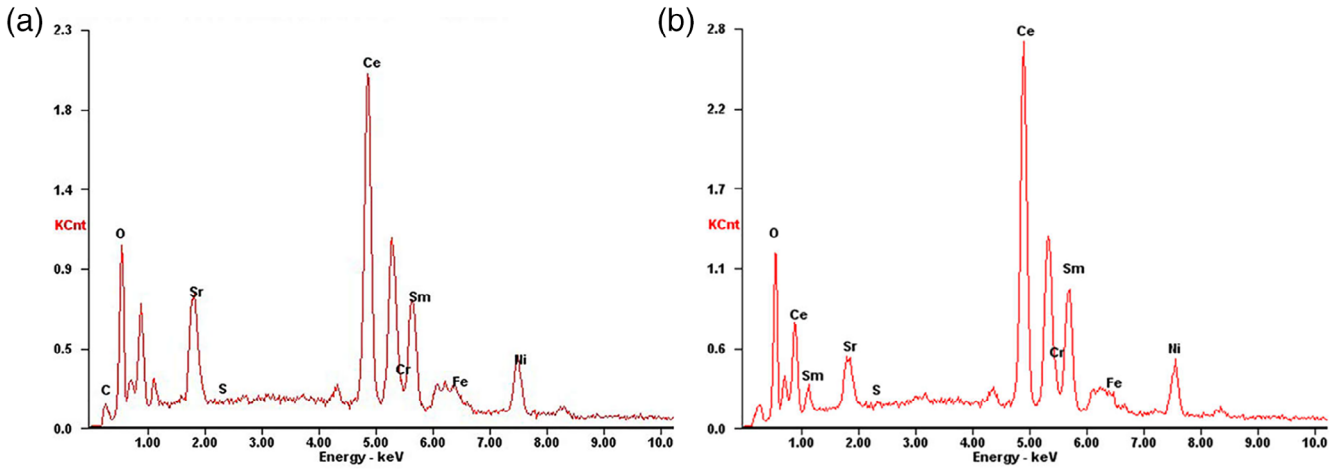

FIGURE 10 EDX results of the Side I (containing H_2S) surface of the spent membranes. (a) M2 after 550 hr operation (containing 200 ppm H_2S) and (b) membrane after 400 hr operation (containing 1,000 ppm H_2S). EDX, energy dispersive X-ray [Color figure can be viewed at wileyonlinelibrary.com]

GEE coal gasifier with a H_2S concentration up to 1,000 ppm (Figure 8b). The membrane maintained stable performance for about 400 hr.

Following the long-term operation, the membrane reactor was stopped for postmortem, as shown in Figures 9, 10, and S2. The catalyst grains on the surface of Side I grew bigger (Figures 9a,c and S2), which indicated the issue of potential catalyst sintering. Further works should be focused on the development of anti-sintering catalysts. The cross-section of the spent M2 (Figure 9b,c) remained intact under various atmospheres. As shown in the EDX results (Figure 10), no sulfur depositions were detected on the surfaces of the membranes and catalysts of the Side I (containing 200 or 1,000 ppm H_2S). Meanwhile, the composition contents of the membranes and catalysts were listed in Tables 1 and 2. No remarkable changes in the compositions of the dense layer and the catalyst layer were found between the fresh and

TABLE 1 The local-area EDX results of the fresh membrane and spent M2 after 550 hr long-term test

	Elements (Atom%)				
Membranes	Sr	Ce	Cr	Sm	Fe
Fresh	9.24	56.46	2.76	17.32	14.22
Spent	10.34	56.09	2.94	16.24	14.40

Abbreviation: EDX, energy dispersive X-ray.

TABLE 2 The local-area EDX results of the fresh and spent catalysts of M2 after 550 hr long-term test

Membranes	Position		Elements (Atom%) Sr	Ce	Cr	Sm	Fe	Ni
Fresh	H_2 side	Surface	1.24	64.74	0	11.29	1.23	21.49
		Cross	1.41	64.35	0	11.83	1.47	20.95
	H_2O side	Surface	8.23	53.86	4.02	17.6	12.19	4.09
		Cross	7.42	52.41	5.09	19.03	12.04	4.00
Spent	H_2 side	Surface	18.05	51.54	0	8.94	4.40	17.05
		Cross	1.95	62.24	0	11.66	4.43	19.73
	H_2O side	Surface	17.2	48.39	4.25	16.62	11.04	2.49
		Cross	6.20	55.71	4.40	17.8	12.62	3.27

Abbreviation: EDX, energy dispersive X-ray.

spent membranes and catalysts. All these results demonstrate the good stabilities of membranes and catalysts in the new IGCC-OTM process.

4 | CONCLUSIONS

In summary, we design a novel OTM-based IGCC concept with CC, denoted by IGCC-OTM. The novel IGCC-OTM process integrated syngas oxidation, H_2 production, and CC in one unit, which simplified the overall process and would decrease the energy penalty. The performance of the membrane reactor was experimentally demonstrated, indicating it met the requirement of this novel process. It is a robust catalytic OTM reactor, made without precious metal elements. The SDC-SSCF membrane and Ni/SDC catalyst exhibit good structure stability in atmospheres containing CO_2, H_2, H_2O(g), and H_2S gases. The effect of catalysts prepared by different methods on hydrogen production performance was investigated. The catalysts prepared by infiltration have better catalytic activity in the hydrogen production process. In addition, this SDC–SSCF membrane exhibits unprecedented stability, high hydrogen production rate, and hydrogen separation factor 10^3–10^4 in the harsh environment of a gas mixture mimicking coal gasification products containing 1,000 ppm H_2S at high temperatures. This IGCC-OTM process shows great potential on CC.

ACKNOWLEDGMENTS

We thank Dr. M. Li and Dr. W. Liu for high-resolution TEM characterizations. L. C., X. Z., and W. Y. thank the financial support from the National Natural Science Foundation of China (21776267 and U1508203), the Strategic Priority Research Program of the Chinese Academy of Sciences (CAS) (XDB17000000), Dalian National Laboratory for Clean Energy (DNL) (DNL180203 and DICP&QIBEBT UN201708), and the Liaoning Revitalization Talents Program (XLYC1801004). X. W. and A. G. would like to thank Exelon Corporation for the cfunding.

ORCID

Xuefeng Zhu https://orcid.org/0000-0001-5932-7620
Weishen Yang https://orcid.org/0000-0001-9615-7421

REFERENCES

1. Davis SJ, Lewis NS, Shaner M, et al. Net-zero emissions energy systems. *Science*. 2018;360:eaas9793.
2. Markewitz P, Kuckshinrichs W, Leitner W, et al. Worldwide innovations in the development of carbon capture technologies and the utilization of CO_2. *Energy Environ Sci*. 2012;5:7281-7305.
3. International Energy Agency (IEA). Energy Technology Perspectives 2017. Accessed December 14 2019. https://www.iea.org/reports/energy-technology-perspectives-2017.
4. Chu S, Majumdar A. Opportunities and challenges for a sustainable energy future. *Nature*. 2012;488:294-303.
5. Karagöz S, Chen HH, Cao MY, Tsotsis TT, Manousiouthakis VI. Multiscale model based design of an energy-intensified novel adsorptive reactor process for the water gas shift reaction. *AIChE J*. 2019;65:e16608.
6. MacDowell N, Florin N, Buchard A, et al. An overview of CO_2 capture technologies. *Energy Environ Sci*. 2010;3:1645-1669.
7. Leung DYC, Caramanna G, Maroto-Valer MM. An overview of current status of carbon dioxide capture and storage technologies. *Renew Sustain Energy Rev*. 2014;39:426-443.
8. Wang M, Lawal A, Stephenson P, Sidders J, Ramshaw C. Post-combustion CO_2 capture with chemical absorption: a state-of-the-art review. *Chem Eng Res Des*. 2011;89:1609-1624.
9. Luis P, Van Gerven T, Van der Bruggen B. Recent developments in membrane-based technologies for CO_2 capture. *Prog Energy Combust Sci*. 2012;38:419-448.
10. Spigarelli BP, Kawatra SK. Opportunities and challenges in carbon dioxide capture. *J CO2 Util*. 2013;1:69-87.
11. Yue MB, Chun Y, Cao Y, Dong X, Zhu JH. CO_2 capture by as-prepared SBA-15 with an occluded organic template. *Adv Funct Mater*. 2006;16:1717-1722.
12. Gelles T, Rezaei F. Diffusion kinetics of CO_2 in amine-impregnated MIL-101, alumina, and silica adsorbents. *AIChE J*. 2019;65:e16785.
13. Sayari A, Belmabkhout Y, Serna-Guerrero R. Flue gas treatment via CO_2 adsorption. *Chem Eng J*. 2011;171:760-774.
14. Lima FV, Daoutidis P, Tsapatsis M. Modeling, optimization, and cost analysis of an IGCC plant with a membrane reactor for carbon capture. *AIChE J*. 2016;62:1568-1580.
15. Tonziello J, Vellini M. Oxygen production technologies for IGCC power plants with CO_2 capture. *Energy Procedia*. 2011;4:637-644.
16. Anantharaman R, Bolland O. Integration of oxygen transport membranes in an IGCC power plant with CO_2 capture. *Chem Eng Trans*. 2011;25:25-30.
17. Rubin ES, Chen C, Rao AB. Cost and performance of fossil fuel power plants with CO_2 capture and storage. *Energy Policy*. 2007;35:4444-4454.
18. Schiebahn S, Riensche E, Weber M, Stolten D. Integration of H_2-selective membrane reactors in the integrated gasification combined cycle for CO_2 separation. *Chem Eng Technol*. 2012;35:555-560.

19. Franz J, Scherer V. An evaluation of CO_2 and H_2 selective polymeric membranes for CO_2 separation in IGCC processes. *J Membr Sci*. 2010;359:173-183.
20. Scholes CA, Kentish SE, Stevens GW. Effects of minor components in carbon dioxide capture using polymeric gas separation membranes. *Sep Purif Rev*. 2009;38:1-44.
21. Escolastico S, Solís C, Kjølseth C, Serra JM. Outstanding hydrogen permeation through CO_2-stable dual-phase ceramic membranes. *Energy Environ Sci*. 2014;7:3736-3746.
22. Wei XT, Kniep J, Lin YS. Hydrogen permeation through terbium doped strontium cerate membranes enabled by presence of reducing gas in the downstream. *J Membr Sci*. 2009;345:201-206.
23. Meng XX, Song J, Yang NT, et al. Ni-$BaCe_{0.95}Tb_{0.05}O_{3-\delta}$ cermet membranes for hydrogen permeation. *J Membr Sci*. 2012;401:300-305.
24. Chen Y, Liao Q, Li Z, et al. A CO_2-stable hollow-fiber membrane with high hydrogen permeation flux. *AIChE J*. 2015;61:1997-2007.
25. Fang SM, Bi L, Yang CL, Yan LT, Chen CS, Liu W. Chemical stability and hydrogen permeation performance of Ni–$BaZr_{0.1}Ce_{0.7}Y_{0.2}O_{3-\delta}$ in an H_2S-containing atmosphere. *J Alloy Compd*. 2009;475:935-939.
26. Cai LL, Li WP, Cao ZW, Zhu XF, Yang WS. Improving oxygen permeation of MIEC membrane reactor by enhancing the electronic conductivity under intermediate-low oxygen partial pressures. *J Membr Sci*. 2016;520:607-615.
27. He ZY, Li CQ, Chen CS, Tong YC, Luo T, Zhan ZL. Membrane-assisted propane partial oxidation for solid oxide fuel cell applications. *J Power Sources*. 2018;392:200-205.
28. Wang HH, Cong Y, Yang WS. High selectivity of oxidative dehydrogenation of ethane to ethylene in an oxygen permeable membrane reactor. *Chem Commun*. 2002;14:1468-1469.
29. Czuprat O, Werth S, Schirrmeister S, Schiestel T, Caro J. Olefin production by a multistep oxidative dehydrogenation in a perovskite hollow-fiber membrane reactor. *ChemCatChem*. 2009;1:401-405.
30. Dong XL, Jin WQ, Xu NP, Li K. Dense ceramic catalytic membranes and membrane reactors for energy and environmental applications. *Chem Commun*. 2011;47:10886-10902.
31. Cao ZW, Jiang HQ, Luo HX, et al. Natural gas to fuels and chemicals: improved methane aromatization in an oxygen-permeable membrane reactor. *Angew Chem Int Ed*. 2013;52:13794-13797.
32. Jiang HQ, Wang HH, Werth S, Schiestel T, Caro J. Simultaneous production of hydrogen and synthesis gas by combining water splitting with partial oxidation of methane in a hollow-fiber membrane reactor. *Angew Chem Int Ed*. 2008;47:9341-9344.
33. Jiang HQ, Wang HH, Liang FY, et al. Improved water dissociation and nitrous oxide decomposition by in situ oxygen removal in perovskite catalytic membrane reactor. *Catal Today*. 2010;156:187-190.
34. Wu X-Y, Ghoniem AF, Uddi M. Enhancing co-production of H_2 and syngas via water splitting and POM on surface-modified oxygen permeable membranes. *AIChE J*. 2016;62:4427-4435.
35. Li WP, Cao ZW, Cai LL, Zhang LX, Zhu XF, Yang WS. H_2S-tolerant oxygen-permeable ceramic membranes for hydrogen separation with a performance comparable to those of palladium-based membranes. *Energy Environ Sci*. 2017;10:101-106.
36. Cai LL, Hu SQ, Cao ZW, Li HB, Zhu XF, Yang WS. Dual-phase membrane reactor for hydrogen separation with high tolerance to CO_2 and H_2S impurities. *AIChE J*. 2019;65:1088-1096.
37. Li WP, Cao ZW, Zhu XF, Yang WS. High-rate hydrogen separation using an MIEC oxygen permeable membrane reactor. *AIChE J*. 2017;63:1278-1286.
38. Cai LL, Zhu Y, Cao ZW, et al. Non-noble metal catalysts coated on oxygen-permeable membrane reactors for hydrogen separation. *J Membr Sci*. 2020;594:117463.
39. Liang WY, Zhou HY, Caro J, Jiang HQ. Methane conversion to syngas and hydrogen in a dual phase $Ce_{0.8}Sm_{0.2}O_{2-\delta}$-$Sr_2Fe_{1.5}Mo_{0.5}O_{5+\delta}$ membrane reactor with improved stability. *Int J Hydrogen Energy*. 2018;43:14478-14485.
40. Li J. OTM-enhanced coal syngas for carbon capture power systems and fuel synthesis applications. DOE/NETL Gasification Systems Program Portfolio Review Meeting, Pittsburgh, PA; March 2017.
41. Zhu XF, Yang WS. Microstructural and interfacial designs of oxygen-permeable membranes for oxygen separation and reaction–separation coupling. *Adv Mater*. 2019;31:1902547.
42. Wang JH, Liu ML. Surface regeneration of sulfur-poisoned Ni surfaces under SOFC operation conditions predicted by first-principles-based thermodynamic calculations. *J Power Sources*. 2008;176:23-30.
43. Duan CC, Kee RJ, Zhu HY, et al. Highly durable, coking and sulfur tolerant, fuel-flexible protonic ceramic fuel cells. *Nature*. 2018;557:217-222.
44. Yang LS, Wang Z, Blinn K, et al. Enhanced sulfur and coking tolerance of a mixed ion conductor for SOFCs: $BaZr_{0.1}Ce_{0.7}Y_{0.2-x}Yb_xO_{3-\delta}$. *Science*. 2009;326:126-129.
45. Ding D, Li XX, Lai SYX, Gerdes K, Liu ML. Enhancing SOFC cathode performance by surface modification through infiltration. *Energy Environ Sci*. 2014;7:552-575.
46. Vohs JM, Gorte RJ. High-performance SOFC cathodes prepared by infiltration. *Adv Mater*. 2009;21:943-956.
47. Su C, Wang W, Liu ML, Tadé MO, Shao ZP. Progress and prospects in symmetrical solid oxide fuel cells with two identical electrodes. *Adv Energy Mater*. 2015;5:1500188.
48. Luo HX, Efimov K, Jiang HQ, Feldhoff A, Wang HH, Caro J. CO_2-stable and cobalt-free dual-phase membrane for oxygen separation. *Angew Chem Int Ed*. 2011;50:759-763.
49. Zhu XF, Liu HY, Cong Y, Yang WS. Novel dual-phase membranes for CO_2 capture via an oxyfuel route. *Chem Commun*. 2012;48:251-253.
50. Bi XX, Meng XX, Liu PY, et al. A novel CO_2-resistant ceramic dual-phase hollow fiber membrane for oxygen separation. *J Membr Sci*. 2017;522:91-99.

SUPPORTING INFORMATION

Additional supporting information may be found online in the Supporting Information section at the end of this article.

How to cite this article: Cai L, Wu X-Y, Zhu X, Ghoniem AF, Yang W. High-performance oxygen transport membrane reactors integrated with IGCC for carbon capture. *AIChE J*. 2020;66:e16247. https://doi.org/10.1002/aic.16247